

Near-Infrared Spectroscopy of Powerful Radio Galaxies at

$$z = 2.2 - 2.6$$

A. S. Evans^{1,2}

Institute for Astronomy, 2680 Woodlawn Drive, Honolulu, HI 96822; ase@astro.caltech.edu

Received _____; accepted _____

arXiv:astro-ph/9802151v1 11 Feb 1998

¹Present Address: Dept. of Astronomy 105-24, California Institute of Technology, Pasadena, CA 91125

²Visiting Astronomer at the United Kingdom Infrared Telescope, which is operated by the Joint Astronomy Centre on behalf of the U.K. Particle Physics and Astronomy Research Council.

ABSTRACT

Near-infrared spectroscopy ($\lambda_{\text{rest}} \sim 3700\text{--}6800 \text{ \AA}$) of eight high redshift powerful radio galaxies (HzPRGs) at $z = 2.2 - 2.6$ is presented. Strong forbidden lines and $\text{H}\alpha$ emission were detected in all sources; the data show evidence that the emission lines of the HzPRGs may contribute a substantial fraction ($\sim 25\text{--}98\%$) of their total observed H - and/or K -band light. Diagnostic emission-line ratios – $[\text{O III}] \lambda 5007 / \text{H}\beta$ vs. $[\text{S II}] \lambda\lambda 6716, 6731 / \text{H}\alpha$ – for three of the eight HzPRGs are consistent with the presence of a Seyfert 2 nucleus; the $[\text{O III}] \lambda 5007 / \text{H}\beta$ and $[\text{S II}] \lambda\lambda 6716, 6731 / \text{H}\alpha$ ratios and/or limits of the remaining five galaxies are inconclusive. Furthermore, all six of the galaxies for which both H - and K -band spectra were obtained have observed $[\text{O III}] \lambda 5007 / (\text{H}\alpha + [\text{N II}] \lambda\lambda 6548, 6583)$ ratios consistent with Seyfert 2 ionization. Much of the inability to detect the weaker emission lines of $[\text{S II}] \lambda\lambda 6716, 6731$ in three of the galaxies and $\text{H}\beta$ in any of the galaxies may be due to moderate amounts of dust: for the two sources with previously measured $\text{Ly}\alpha$ fluxes, the observed $\text{Ly}\alpha / \text{H}\alpha$ ratios are ~ 1.5 , much less than the value of 16 expected for gas in a dust-free medium photoionized by a hard, nonthermal continuum. If such a discrepancy is due solely to dust, this ratio translates into $A_V \sim 0.5\text{--}1.0$ mag (depending on which extinction curve – Milky Way, SMC, LMC – is used) at the rest-frame optical wavelengths of the galaxies, and a corresponding factor of $\sim 1.6\text{--}2.5$ reduction in optical flux.

None of the eight HzPRGs at $z = 2.2 - 2.6$ HzPRGs have broad ($\Delta v_{\text{FWHM}} > 1500 \text{ km s}^{-1}$) emission-line cores, and it is not clear whether any have broad emission-line wings. However, the near-infrared spectrum of 3C 22, a $z = 0.937$ radio galaxy with $1 \mu\text{m}$ luminosity comparable to that of the radio galaxies at $z = 2.2 - 2.6$ and a radio luminosity only 3–5 times less, shows

direct evidence for broad H α emission wings. Such a feature is indicative of the presence of a partially obscured Seyfert 1 nucleus. Given that 3C 22 is at $\sim 1/3$ the luminosity distance of the sample of HzPRGs at $z = 2.2 - 2.6$, a thorough search for such a faint feature in the more distant galaxies may require 8–10 meter-class telescopes.

These new data, along with recent UV-to-optical polarimetry showing evidence of high polarization in many HzPRGs, provide evidence that many HzPRGs are predominantly ionized by an active nucleus, and that a significant fraction of their SED may be due to non-thermal emission from an active galactic nucleus.

Subject headings: galaxies: active—galaxies: ISM

1. Introduction

High redshift powerful radio galaxies (HzPRGs: $P_{408\text{MHz}} > 10^{27} h^{-2} \text{ W Hz}^{-1}$, $z \gtrsim 1$)³ are potentially an important probe of galaxy evolution at early epochs. The recent detections of strong emission lines from HzPRGs at observed near-infrared wavelengths (e.g., Rawlings, Eales, & Lacy 1991; McCarthy, Elston, & Eisenhardt 1992; Eales & Rawlings 1993, 1996) has provided a new diagnostic tool with which to study these objects, although the nature of line emission in HzPRGs is currently a subject of great debate. Part of the difficulty in interpreting line emission in HzPRGs has been that the use of standard optical diagnostic emission-line ratios (e.g. Baldwin, Phillips, & Terlevich 1981; Veilleux & Osterbrock 1987), commonly used to differentiate between thermal ionization and low or high-excitation ionization from a non-thermal source, has until recently been problematic because rest-frame optical emission from galaxies at $z > 1$ is redshifted to near-infrared wavelengths at current epochs.

A new generation of infrared spectrographs has now made it possible to begin systematic studies of the dominant ionization mechanisms in HzPRGs via their rest-frame optical emission-line spectra. In particular, the new *K*-band spectrograph (KSPEC: Hodapp et al. 1994) on the University of Hawaii (UH) 2.2 m telescope on Mauna Kea provides the unique capability of simultaneous coverage of the $\sim 1.0\text{--}2.4 \mu\text{m}$ wavelength band at typical spectral resolution $\lambda / \Delta\lambda \sim 700$, while the infrared spectrograph (CGS4) on the 3.8 m United Kingdom Infrared Telescope (UKIRT) on Mauna Kea can provide coverage of either the full *J*, *H*, or *K*-band near-infrared windows at a spectral resolution of $\lambda / \Delta\lambda \sim 860$.

A nearly complete sample of HzPRGs in the redshift range $z = 2.2 - 2.6$ has been selected. An attempt has been made, insomuch as possible, to obtain near-infrared spectra

³Throughout this paper, $H_o = 100h \text{ km s}^{-1} \text{ Mpc}^{-1}$ and $q_o = 0.5$ are assumed.

with similar sensitivity and coverage in rest-frame wavelength. The choice of the redshift range and wavelength coverage was designed to maximize the number of rest-frame optical diagnostic lines observed. As far as the author is aware, this is the first such study that obtains both H - and K -band spectra for a fairly complete sample of HzPRGs.

The outline of this paper is as follows: Sample selection and observing procedures are discussed in § 2 and § 3 respectively. Data reduction methods are summarized in § 4. The discussion in § 5 focuses on the observed emission-line spectra and calculated extinction in the HzPRGs, as well as on how the properties of HzPRGs compare with the properties of local radio galaxies, and optically selected Seyferts, LINERs, and H II region-like galaxies.

2. Sample Selection

The study of HzPRGs at near-infrared wavelengths from the ground is optimized for redshifts in the range $z \sim 2.2 - 2.6$ which simultaneously places the largest number of rest-frame optical diagnostic emission lines (e.g. $H\beta$, $[\text{O III}] \lambda 5007$, $H\alpha$, $[\text{N II}] \lambda\lambda 6548, 6583$, and $[\text{S II}] \lambda\lambda 6716, 6731$ - hereafter $[\text{S II}] \lambda 6724$) directly in the H -band and K -band atmospheric windows. When this project was started in early 1993, relatively few HzPRGs were in the literature with redshifts in this range and with $\delta > 0^\circ$ (as required by this study for ease in observing from Mauna Kea). Nine galaxies were ultimately selected - five of these objects (B3 0731+438, 3C 257, 53W002, MG 1744+18, and 4C 40.36) were selected from a list compiled by Eales & Rawlings (1993), who presented observed K -band spectra of HzPRGs with relatively low sensitivity, and four (TX 0200+015, TX 0828+193, 4C 48.48, and 4C 23.56) were selected from the ultra-steep spectrum (USS) radio galaxy survey (e.g., Röttgering 1993; van Ojik 1995; Röttgering et al. 1995; Chambers et al. 1996). With the exception of 53W002, all of these HzPRGs were observed as part of this survey. The positions and redshifts of the eight observed sources are listed in Table 1.

The final observing list included one additional object, 3C 22, which was added during the very first phases of this study. The galaxy 3C 22 has a $1\ \mu\text{m}$ luminosity comparable to the other eight HzPRGs in the sample, and a radio luminosity only 3–5 times fainter, however it has a redshift ($z \sim 0.94$) only approximately half that of the others. It was originally included in the list mainly as a hedge against the possibility that most of the higher redshift objects would be too faint for obtaining spectra with the signal-to-noise ratio necessary to make reasonable measurements of emission-line ratios. If this had indeed turned out to be the case, a more limited spectroscopic study of HzPRGs at redshifts $z \sim 1$ would have been carried out. However, both KSPEC and CGS4 provided sufficient sensitivity for studying the $z = 2.2 - 2.6$ sources, although the data obtained for 3C 22 did have a significantly higher signal-to-noise ratio than all of the other sources. The data for 3C 22 is therefore interesting in its own right as an example of how the data for the higher redshift sources might appear if higher sensitivity near-infrared data is eventually obtained.

3. Observations

In planning the observations of the sample of HzPRGs, the first priority was to obtain simultaneous H -band and K -band spectra with KSPEC, and then to obtain H -band and K -band spectra using CGS4 of those sources that, for whatever reason, could not successfully be observed with KSPEC. In the end, due to weather and equipment availability, three sources were observed with both spectrometers and five with CGS4 alone. The galaxy 3C 22 was observed only with KSPEC.

Table 1 presents a complete journal of the near-infrared observations. K -band spectra were obtained of eight HzPRGs with better sensitivity than any previously published K -band data, H -band spectra were obtained for five sources, and one object was also observed at J -band. Except for the recent publication of H -band data for one source, these

are the first *H*-band and *J*-band spectra of HzPRGs in this redshift range published to date. Observing parameters are also listed in Table 1. Details of the observing procedures at each of the two telescopes used are discussed separately below.

3.1. UH 2.2m Telescope

Observations with the infrared spectrograph, KSPEC (Hodapp et al. 1994), on the UH 2.2m Telescope were made during four observing periods between 1993 July and 1994 December. KSPEC is a cross-dispersed echelle spectrograph configured to cover the wavelength range 1.1–2.5 μm in three orders (*J*, *H*, and *K*) on a 256 \times 256 NICMOS-3 HgCdTe detector array. The wavelength resolutions (at 2.2 μm) for each of the observations are listed in Table 1. Additionally, the wavelength range 0.7–1.0 μm is also dispersed in several orders on the array. However, the order crowding at 0.7–1.0 μm is such that only spectra of point-like sources can effectively be extracted, and this wavelength range is also compromised due to the fact that KSPEC is only in focus at $\lambda > 0.85 \mu\text{m}$. In addition to its spectral capabilities, KSPEC also provides simultaneous imaging of approximately one square arcminute of sky around the slit on a second NICMOS-3 array. For the 1994 December observing period, the new UH tip-tilt system (Jim et al. 1997) was also implemented, notably improving the tracking, offsetting, and seeing of the observations and data.

For the 1995 November observing period, an upgraded version of KSPEC was used in combination with the UH tip-tilt system. The new device uses a HAWAII 1024 \times 1024 HgCdTe array as the spectral detector, and provides coverage over the wavelength range 0.81–2.54 μm without confusion due to overlapping orders.

Each observing night began with a series of dome flats with incandescent lights turned

on, then off. Once the telescope was guiding with the source in the slit, a 180 sec exposure was taken, followed by a second 180 sec exposure with the slit positioned $10''$ off-source. For all observations, except during 1995 November, each spectrum exposure was accompanied by a 140 sec image exposure. No image exposures were taken for the 1995 November observations except to occasionally check the position of stars in the field. For observations prior to 1994 December, the observing pattern was source-sky-source-sky ..., but the pattern was changed to source-sky-sky-source ... for the 1994 December observations to minimize spurious features created by changing sky conditions. Observations of standard AV stars near each source were made for flux calibration and to remove telluric lines. Observations of an argon lamp were used for wavelength calibration.

3.2. United Kingdom 3.8m Infrared Telescope

Observations were made with the infrared spectrometer CGS4 on UKIRT during the observing periods 1993 August, 5–9 and 1994, October 3–7 . CGS4 is a $1\text{--}5\ \mu\text{m}$ 2D grating spectrometer with a 58×62 InSb array. For all observations, a $75\ \text{line mm}^{-1}$ grating was used in first order. The wavelength resolutions and sampling scheme used for each source is listed in Table 1. For most sources, sampling was done over 2 pixels in 6 or 8 steps in the wavelength direction. A one pixel-wide ($1.5''$) slit was used for all observations.

Observations with an upgraded version of CGS4 were made during four observing periods from 1995, May to 1996, April. The 1995, May observations were done under shared-risk time. The new detector was a 256×256 InSb array. A $75\ \text{line mm}^{-1}$ grating in first order was used for the first three observing periods, and a $150\ \text{line mm}^{-1}$ grating in first order was used for the last observing period. A one pixel-wide ($1.2''$) slit was used for all observations except for the B30731+438 and 3C 257 observations which were obtained using a two pixel-wide $2.5''$ slit.

Spectral data were taken using exposure times between 60 to 540 sec, with 20 to 90 sec of each exposure made at each detector position during the sampling. The slit was then moved 15"–30" in the spatial direction on the array for the next multi-sampling exposure. Thus, the source appears on the array as a positive and negative spectrum after the first frame is subtracted from the second. The source-sky observation sequence was the same as that used in the 1994, December KSPEC observations. Flux calibrations were again made using AV standard stars located near each source, and a krypton lamp was used for wavelength calibration.

For the 1995 May observations of MG 1744+18, a problem was encountered; the source flux of the positive spectrum was more than that of the negative spectrum flux, implying that the source was only partially in the slit in the second position. Alternatively, the flux of the positive A star spectrum was less than the negative spectrum flux. The slit also appeared to be tilted relative to the array as evident by the position of the OH sky lines. Because of this, only half the data had enough flux to be usable, and no photometry was possible for MG 1744+18.

4. Results

All data reduction was done within IRAF. For KSPEC data the procedure was as follows: Sky frames were first subtracted from the source frames. The result was then divided by an appropriate flat field and then averaged. Since there were only a few bad pixels, and none were on the spectral area containing the source spectrum, the bad pixels were individually set to zero before the spectral orders were extracted with the APALL package. The extracted spectra were then wavelength calibrated and divided by the standard star spectrum (which had been averaged, flatfielded, and extracted in the same manner as the source spectrum) to remove any instrumental effects and atmospheric lines.

Because of the narrow width of the slit, no photometry was determined for any of the KSPEC observations. Finally the spectrum was multiplied by a Planck blackbody spectrum with the same temperature as the standard star. The CGS4 data were reduced in a same manner as the KSPEC data, except that flat fielding and masking of bad pixels was done automatically after each observation. Photometry was determined for all galaxies except B3 0731+438, which was observed at the end of a observing period of variable weather, and MG 1744+18 (see §3.2).

The near-infrared spectra for all eight HzPRGs at $z = 2.2 - 2.6$ that were observed are plotted in Figure 1. Measured emission-line properties are summarized in Table 2. For most of the sources, [O III] $\lambda\lambda$ 4959, 5007, $H\alpha$ + [N II] $\lambda\lambda$ 6548, 6583, and [S II] λ 6724 were detected. The emission line [O II] λ 3727 was also detected in 4C 48.48. $H\beta$ and [O I] λ 6300 were not detected in any of the HzPRGs. Taking into account the signal-to-noise ratio of any individual galaxy spectrum, all of the HzPRG emission-line spectra plotted in Figure 1 (with the exception of the anomalous source TX 0828+193SW) look similar, and the lines have similar widths.

For 4C 23.56 there is a discrepancy in the $H\alpha$ flux measured from two separate observing periods. During the 1993, August observations, the telescope was positioned on the source by offsetting from a nearby, faint star. For the 1994, October observations, the telescope was first peaked-up on a relatively nearby star whose position is known to high accuracy, then the telescope was slewed to the radio coordinates of the source. Because the $H\alpha$ flux measured in the latter observations is three times stronger than the line measured in the former, the position uncertainty of the faint offset star is most likely a large fraction of the slit width and the 1993, August data will be ignored in further discussion of this source.

For 4C 40.36 the observing conditions were variable for the period the data were

obtained. Photometry for the standard star (HD 166208) observed during the night in question was compared to the standards (BS 7503 and BS 8143) observed on the two photometric nights, and the flux of HD 166208 was found to be 20% lower than the flux expected under photometric conditions. The spectrum in Figure 1 and the emission-line flux values in Table 2 for 4C 40.36 have been scaled appropriately to take this factor into account.

Figure 2 shows the spectrum of the lower redshift radio galaxy 3C 22 that was obtained during 1994, December. The signal-to-noise ratio of this spectrum is significantly better than that of the objects in Figure 1. The $H\alpha+[N\ II]\ \lambda\lambda 6548, 6583$ line wings for 3C 22 are remarkably broad, characteristic of Seyfert 1 galaxies. Emission-line ratios for 3C 22 are also summarized in Table 2, but their discussion will be postponed until after the discussion of the higher redshift objects.

Several of these sources have been observed by others (McCarthy et al. 1992; Eales & Rawlings 1993, 1996). Of the two HzPRGs for which photometric values can be compared with previous measurements, the $H\alpha+[N\ II]\ \lambda\lambda 6548, 6583$ flux value of $2.9 \times 10^{-18}\ \text{W m}^{-2}$ reported by Eales & Rawlings (1996) for 3C 257 agrees well with the value of $2.6 \times 10^{-18}\ \text{W m}^{-2}$ in Table 2, while the value of $3.4 \times 10^{-18}\ \text{W m}^{-2}$ for 4C 40.36 (Table 2) is higher than value of $2.6 \times 10^{-18}\ \text{W m}^{-2}$ reported by Eales & Rawlings (1993). The Eales & Rawlings (1993, 1996) observations made use of a $3'' \times 3''$ aperture, thus the agreement in 3C 257 line flux and lack of agreement in 4C 40.36 line flux may indicate that the $H\alpha+[N\ II]\ \lambda\lambda 6548, 6583$ emission-line region of 3C 257 is compact and that of 4C 40.36 is extended, or that the $H\alpha+[N\ II]\ \lambda\lambda 6548, 6583$ flux for 4C 40.36 presented in this paper is an overestimate. The resolution, sampling, and integration times (Table 1) for the spectra presented in this paper have allowed for a better determination of rest-frame optical line profiles of $z > 2$ HzPRGs than previously published. In addition, the $H\alpha+[N\ II]\ \lambda\lambda 6548, 6583$ profile of

3C 22 (Figure 2) is consistent with recently published data of this source (Economou et al. 1995; Rawlings et al. 1995).

5. Discussion

5.1. Emission-Line Diagnostics

Figure 3 shows the $\log ([\text{O III}] \lambda 5007 / \text{H}\beta)$ vs. $\log ([\text{S II}] \lambda 6724 / \text{H}\alpha)$ diagram commonly used to distinguish between galaxies with Seyfert, LINER, and H II-region emission-line spectra. Emission from $[\text{S II}] \lambda 6724$ can emanate from ionized hydrogen regions, as well as from semi-ionized regions where collisional ionization is significant. Enhancement of forbidden lines such as $[\text{O I}] \lambda 6300$, $[\text{N II}] \lambda\lambda 6548, 6583$, and $[\text{S II}] \lambda 6724$ occurs in AGNs because, unlike H II regions, they have extended partially-ionized zones created by an excess of X-rays (the absorption cross sections of neutral hydrogen, helium and all ions are small for X-rays, thus X-rays tend to escape the ionized region before interacting: Veilleux & Osterbrock 1987). $[\text{O III}] \lambda 5007$ is a high ionization line photoionized by UV photons, and thus tends to be strong in Seyfert galaxies.

Instead of attempting to determine the relative contributions of $\text{H}\alpha$ and the $[\text{N II}] \lambda\lambda 6548, 6583$ doublet to the blended $\text{H}\alpha + [\text{N II}] \lambda\lambda 6548, 6583$ complex, the smallest ratio of $[\text{N II}] \lambda 6583 / \text{H}\alpha$ ($= 0.19$) observed for a sample of luminous infrared galaxies (Kim et al. 1995) has been adopted and plotted (large circles with embedded numerals) for all of the HzPRGs in the sample⁴. Choosing such a ratio tends to bias the data towards the H II-region portion of the diagram. To illustrate the extent to which the data are

⁴ It is unlikely, given the widths of the $[\text{O III}] \lambda 5007$ lines, that the $\text{H}\alpha + [\text{N II}] \lambda\lambda 6548, 6583$ complexes are pure $\text{H}\alpha$. However, if the complexes were purely $\text{H}\alpha$, their observed breadth ($\Delta v_{\text{FWHM}} \gtrsim 1000 \text{ km s}^{-1}$) would be evidence against H II region-like emission.

affected by this ratio, the values that result from assuming $[\text{N II}] \lambda 6583 / \text{H}\alpha = 1.0$, the value adopted by Eales & Rawlings (1993) based on the predictions of photoionization models and the observed value for low-redshift powerful radio galaxies (LzPRGs), and $[\text{N II}] \lambda 6583 / \text{H}\alpha = 3.74$, the largest value observed by Kim et al. (1995), have also been plotted as small, filled-in circles. Note that in all of the H -band spectra except for the spectrum of 4C 48.48, the estimated $\text{H}\beta$ upper limits (3σ) provide weak constraints on the lower limit of $[\text{O III}] \lambda 5007 / \text{H}\beta$. Thus, in all sources except 4C 48.48 and 4C 40.36, the $[\text{O III}] \lambda 5007 / \text{H}\beta$ ratio is determined assuming $\text{H}\alpha / \text{H}\beta \geq 3$, and thus $[\text{O III}] \lambda 5007 / \text{H}\beta \geq 3 \times [\text{O III}] \lambda 5007 / \text{H}\alpha$ (the upper limit for $[\text{O III}] \lambda 5007 / \text{H}\beta$ in 4C 40.36 is taken from Iwamuro et al. 1996). Three of the eight HzPRGs plotted in Figure 3 clearly fall in the Seyfert region of the plot. The $[\text{O III}] \lambda 5007 / \text{H}\beta$ and $[\text{S II}] \lambda 6724 / \text{H}\alpha$ ratios and/or limits for TX 0200+015, TX 0828+193, 3C 257, MG 1744+18, and 4C 23.56 are inconclusive.

Additional information about the ionization mechanism is obtained by examining the $[\text{O III}] \lambda 5007 / (\text{H}\alpha + [\text{N II}] \lambda\lambda 6548, 6583)$ ratios. Table 3 lists the average value for this ratio as a function of emission-line classification for galaxies in the *IRAS* Bright Galaxy Sample (BGS) and a sample of “warm” *IRAS* galaxies (Kim et al. 1995; Veilleux et al. 1995), as well as for a sample of LzPRGs with Seyfert 2 emission-line spectra (i.e., Cygnus A: Osterbrock & Miller 1975; PKS 1345+12: Grandi 1977; 3C98, 3C192, 3C327: Costero & Osterbrock 1977). Despite the obvious scatter due presumably to extinction and possible metallicity effects, the ratio provides a notable separation between Seyfert galaxies and those of the H II and LINER class. A comparison of these low-redshift, active galaxies with the six HzPRGs at $z = 2.2 - 2.6$ for which both H - and K -band spectra have been obtained show all six HzPRGs to have $[\text{O III}] \lambda 5007 / (\text{H}\alpha + [\text{N II}] \lambda\lambda 6548, 6583)$ ratios consistent with Seyfert 2 galaxies⁵. The average value of the $[\text{O III}] \lambda 5007 / (\text{H}\alpha + [\text{N II}]$

⁵The $[\text{O III}] \lambda 5007$ measurement of 4C 40.36 by Iwamuro et al. (1996), obtained with a

$\lambda\lambda 6548, 6583$) ratio for these six HzPRGs is also listed in Table 3. Thus, the dominant source of ionization for these galaxies appears to be no different from that observed in most low-redshift, narrow-line radio galaxies.

Because the $H\alpha$ and $[\text{N II}] \lambda\lambda 6548, 6583$ lines are blended, a direct comparison of the low ionization-to- $H\alpha$ line ratio of these high-redshift galaxies to their low-redshift counterparts cannot be made. An alternative is to compare the $[\text{S II}] \lambda 6724 / (H\alpha + [\text{N II}] \lambda\lambda 6548, 6583)$ ratio. For the 5 HzPRGs with $[\text{S II}] \lambda 6724$ detections, $[\text{S II}] \lambda 6724 / (H\alpha + [\text{N II}] \lambda\lambda 6548, 6583) = 0.25 \pm 0.07$, similar to the mean value of 0.27 ± 0.05 observed for a sample of LzPRGs with Seyfert 2 emission-line spectra. Changes in properties such as the elemental abundances of the host galaxy, the shape of the ionizing spectrum, and the electron density of the gas being ionized will act to vary this ratio (note that extinction has little effect on this ratio because these emission lines have similar wavelengths). Table 3 contains a summary of average $[\text{S II}] \lambda 6724 / (H\alpha + [\text{N II}] \lambda\lambda 6548, 6583)$, $H\alpha / [\text{S II}] \lambda 6724$, $H\alpha / [\text{N II}] \lambda\lambda 6548, 6583$, and $[\text{N II}] \lambda\lambda 6548, 6583 / [\text{S II}] \lambda 6724$ ratios as a function of emission-line classification. Essentially, $[\text{S II}] \lambda 6724 / (H\alpha + [\text{N II}] \lambda\lambda 6548, 6583)$ is a function of $H\alpha / [\text{S II}] \lambda 6724$ and $[\text{N II}] \lambda\lambda 6548, 6583 / [\text{S II}] \lambda 6724$, where $H\alpha / [\text{S II}] \lambda 6724$ appears to account for most of the variation in the average. On average, $[\text{S II}] \lambda 6724 / (H\alpha + [\text{N II}] \lambda\lambda 6548, 6583)$ is larger for LINERs and Seyfert 2 galaxies than in H II region-like galaxies (see Table 3), in part because the former have more extended semi-ionized regions (i.e., $H\alpha / [\text{S II}] \lambda 6724$ decreases as the extent of the semi-ionized region increases). Variations in the metal abundance in the galaxies in the sample undoubtedly contribute to the scatter.

$PA = 0$ and a $1.5'' \times 60''$ aperture, is included because their H -band image shows most of the flux to be within $1.5''$ of the center of the galaxy. The $[\text{O III}] \lambda 5007$ flux is $3.86 \times 10^{-18} \text{ W m}^{-2}$, and thus the observed $[\text{O III}] \lambda 5007 / H\alpha + [\text{N II}] \lambda\lambda 6548, 6583$ ratio for 4C 40.36 is 1.1.

For example, a substantial decrease in the metal abundance would cause a substantial decrease in $[\text{S II}] \lambda 6724 / (\text{H}\alpha + [\text{N II}] \lambda\lambda 6548, 6583)$ (i.e., $\text{H}\alpha / [\text{S II}] \lambda 6724$ increases as the metal abundance decreases), and vice versa. The observation that LzPRGs and HzPRGs have similar $[\text{S II}] \lambda 6724 / (\text{H}\alpha + [\text{N II}] \lambda\lambda 6548, 6583)$ ratios may indicate that, even though HzPRGs are at substantially higher lookback times and possess higher radio luminosities, the properties of the ionizing source and the ionized gas are similar.

It is worthwhile to consider whether the gas in the HzPRGs could be ionized by supernova remnants (SNRs). Indeed, there are a few SNRs that exhibit emission-line ratios similar to Seyfert 2 galaxies. A conservative estimate of the SNR rate required to explain the observed emission lines can be determined by considering the extreme SNR in NGC 6946, which has $\log([\text{O III}] \lambda 5007 / \text{H}\beta) = 0.85$ and $\log([\text{S II}] \lambda 6724 / \text{H}\alpha) = -0.06$ (Blair & Fesen 1994). The flux in the $[\text{O III}] \lambda 5007$ line is 2.5×10^{-17} Watts m^{-2} . At a distance corresponding to $z = 2.4$, the SNR would have a flux of $\sim 2.5 \times 10^{-17} (5.1 \text{ Mpc} / 9330h^{-1} \text{ Mpc})^2 = 7.5 \times 10^{-24} h^2$ Watts m^{-2} . Thus, to produce the average $[\text{O III}] \lambda 5007$ flux (i.e. 3×10^{-18} Watts m^{-2}) observed in the HzPRGs in the sample would require $4 \times 10^5 h^{-2}$ SNRs. Adopting a conservative estimate of 5000 yr for the SNR lifetime, HzPRGs would have to produce SNRs at an implausible rate of $80h^{-2} \text{ yr}^{-1}$ to maintain their $[\text{O III}] \lambda 5007$ flux.

5.2. $L_{[\text{O III}] \lambda\lambda 4959, 5007}$ vs. $P_{151\text{MHz}}$

Previous authors have used the $[\text{O III}] \lambda\lambda 4959, 5007$ luminosity versus the observed 151 MHz radio power for HzPRGs in an attempt to infer a causal relationship between the ionization source for the gas and the source of the radio emission. Rawlings et al. (1989) have compiled data primarily for LzPRGs, and more recently, Eales & Rawlings (1993, 1996) have added data for HzPRGs. Figure 4a is a plot adapted from Eales & Rawlings

(1996) of the [O III] $\lambda\lambda 4959, 5007$ luminosity versus the observed 151 MHz radio power for an unbiased 3C sample of FR II radio galaxies with $z < 0.5$ and a collection of HzPRGs. Data for the HzPRGs TX 0200+015, B3 0731+438, TX 0828+193, 4C 48.48, and 4C 23.56 have also been plotted.

A simple interpretation of Figure 4a would be that there appears to be a correlation between the [O III] $\lambda\lambda 4959, 5007$ emission-line luminosity and the radio power (such a correlation would appear to be even tighter perhaps for the HzPRGs than for the LzPRGs), and that a common excitation source (e.g. the central AGN) is responsible for both. However, the real answer is clearly not so simple. The apparent strong correlation between the [O III] $\lambda\lambda 4959, 5007$ emission-line luminosity and the radio power, $P_{151\text{MHz}}$, in Figure 4a is almost entirely an artifact of distance, as evidence by the plot of the ratio $L_{[\text{OIII}]\lambda\lambda 4959,5007}/P_{151\text{MHz}}$ vs. $P_{151\text{MHz}}$ (Figure 4b) which shows no correlation in the sample as a whole. However, note the apparent strong correlation exhibited in Figure 4b by the HzPRGs (i.e., all sources with $P_{151\text{MHz}} > 10^{27} \text{ W Hz}^{-1} \text{ sr}^{-1}$ and $L_{[\text{OIII}]\lambda\lambda 4959,5007}/P_{151\text{MHz}} > 10^8$). Indeed, for the most powerful radio galaxies at $z > 0.5$ the morphology of the emission-line gas is aligned with the radio axis (McCarthy et al. 1987), which suggests that a correlation between the two quantities exists.

The extraordinary strength of the emission lines in HzPRGs is also evident from the data in Table 4: of the TX and 4C galaxies in the sample for which high signal-to-noise ratio H - or K -band magnitudes were made available from Keck imaging (L. Armus, private communication), the emission lines appear to contribute anywhere between 25–98% of the broad-band near-infrared light. These percentages are substantially higher than those observed in the most powerful radio galaxies in the local Universe, but are consistent with other HzPRGs with published near-infrared spectra (McCarthy et al. 1992; Eales & Rawlings 1993, 1996). Such high emission-line luminosities illustrate the danger of

interpreting the magnitudes and morphologies of high radio-power galaxies as being purely stellar in origin (see Eales & Rawlings 1993, 1996 for discussions on this issue). Evidence for possible AGN contamination of the broad-band morphologies of high radio-power galaxies has been demonstrated by Dunlop & Peacock (1993), who show that the rest-frame $1.1 \mu\text{m}$ flux of a sample of 3CR galaxies tend to be more extended and aligned with the radio axis than a sample of lower radio-power Parkes galaxies in the same redshift range ($z \sim 1$). Such extended and aligned morphologies are more pronounced at rest-frame UV wavelengths and are undoubtedly connected with the energetics of the central engine, and/or due to an optically-thick, circumnuclear dust/gas torus extinguishing light perpendicular to the radio axis. Rest-frame UV spectropolarimetry (Dey & Spinrad 1995; Cimatti et al. 1996; Manzini & di Serego Alighieri 1996 and references therein) and optical imaging polarimetry (Knopp & Chambers 1997; Knopp 1997), show further evidence of AGN contamination of broad-band light in many HzPRGs.⁶ Indeed, four of the galaxies discussed in this paper (TX 0200+015, B3 0731+438, TX 0828+193, and 4C 23.56) show rest-frame optical polarizations of 10–45% (Knopp & Chambers 1997; Knopp 1997), indicating that a significant fraction of the rest-frame UV-to-optical continuum emission from many HzPRGs may be scattered/reprocessed AGN light.

5.3. TX 0828+193SW: A Component Dominated by Continuum-Emission

In some HzPRGs, there appear to be “components” that are genuinely dominated by continuum emission at observed optical and near-infrared wavelengths. Figure 1 shows two extractions of the southwestern “component” of TX 0828+193. Unlike the northeastern

⁶There is one example of an HzPRG, 4C 41.17 at $z = 3.8$, that does not appear to have polarized UV light (Dey et al. 1997).

component, TX 0828+193SW has no notable strong emission lines, but has comparatively strong continuum emission. Spectroscopy of the radio galaxy at wavelengths near 4000 Å (observer-frame) reveals strong Ly α , C IV, He II, and C III] emission lines in the NE component, but no emission lines in the SW component (van Ojik 1995; Röttgering et al. 1997). Radio, *R*-band imaging data, and near-infrared imaging data taken of TX 0828+193 show the radio core to be coincident with the NE component and the SW component to lie $\sim 5''$ away from the radio core, but still along the radio axis of the galaxy (Röttgering et al. 1995; Knopp & Chambers 1997; see Figure 5 in the Appendix). This raises the possibility that either TX 0828+193SW is a cloud being illuminated by continuum emission emanating from TX 0828+193NE, or that a buried AGN residing in TX 0828+193SW is ionizing gas in TX 0828+193NE. The two best examples of ionization of off-nuclear knots in low-redshift radio galaxies are Coma A (van Breugel et al. 1985) and PKS 2152-69 (Tadhunter et al. 1987). In the case of Coma A, the nuclear region has strong continuum emission and relatively weak lines, whereas the off-nuclear knot has relatively strong line emission. In the case of PKS 2152-69, both the nucleus and the off-nuclear knot have notable continuum emission, but the line emission from the off-nuclear knot, especially [O III] λ 5007, is stronger. Such data would imply that the AGN is in TX 0828+193SW and is ionizing the northeastern component. Recent multi-wavelength, broad-band polarimetry measurements of TX 0828+193 show evidence for TX 0828+193NE having polarization consistent with scattering due to dust (Knopp & Chambers 1997).

Because TX 0828+193SW has no emission-line or absorption features from which its redshift can be determined, there exists the possibility that it is simply an unrelated object along the line of sight. Though the chance of such a superposition is low, there is precedent for concern, most notably the foreground star coincident with 3C368 (Hammer, Le Fèvre, & Proust 1991). In the recently discovered HzPRG MG 1019+0535, a double-component morphology is observed, one component of which shows no sign of strong line emission

(Dey, Spinrad, & Dickinson 1995). The authors argue strongly in favor of the lineless component being a foreground object, but unlike TX0828+193, the two ‘components’ of MG 1019+0535 are orthogonal to the radio axis. Given the geometry of TX0828+193, the polarimetry measurements, and that such double-component structures aligned with the radio axis are observed in other radio galaxies (e.g. MRC 0406-24: Eales & Rawlings 1993), TX0828+193SW is most likely at the redshift of the radio source.

5.4. Dust

The evidence to date that HzPRGs as a class contain substantial amounts of dust is mixed, but compelling - while polarimetry observations show evidence for scattering by dust in several HzPRGs (Dey & Spinrad 1995; Cimatti et al. 1996; Manzini & di Serego Alighieri 1996 and references therein; Knopp & Chambers 1997; Knopp 1997), far-infrared/submillimeter bolometry (Golombek, Miley, & Neugebauer 1988; Evans et al. 1996; Dunlop et al. 1994; Chini & Kreugel 1994; Ivison 1995; Hughes, Dunlop, & Rawlings 1997) and CO spectroscopy (Evans et al. 1996; Downes et al. 1996; van Ojik et al. 1997a; Scoville et al. 1997) surveys of HzPRG show evidence for substantial amounts of dust in only a few sources. Regardless of whether or not HzPRGs have comparable or more dust as that inferred by the SEDs and molecular gas masses of many low-redshift radio galaxies (e.g, Golombek, Miley, & Neugebauer 1988; Mirabel, Sanders & Kazès 1989; Knapp & Patten 1991; Impey & Gregorini 1993; Mazzarella et al. 1993; Evans 1996), only moderate amounts are required to notably decrease the observed flux of the optical (rest-frame) emission lines and continuum. Specifically, the extinction in the HzPRGs may be substantial enough such that the weaker lines of $H\beta$, $[O\ I]\ \lambda 6300$, and $[S\ II]\ \lambda 6724$, and possible features such as emission-line wings (see §5.5), fall below the detection threshold of the spectra in Figure 1.

Estimates of extinction in HzPRGs in the sample were made by comparing the

observed line ratios of hydrogen recombination lines with their intrinsic ratio (i.e., ratios in a dust-free environment). Intrinsic ratios for low-density gas photoionized by a thermal continuum source are $H\alpha/H\beta = 2.85$ and $Ly\alpha/H\alpha = 8.10$ (Osterbrock 1989). However, because the evidence presented here and elsewhere (see McCarthy 1993) implies that gas in HzPRGs is heated by a hard nonthermal continuum, enhanced $Ly\alpha$ and $H\alpha$ emission in predominantly neutral regions heated by X-rays must be taken into account (note that collisions resulting in the emission of $Ly\alpha$ and $H\alpha$ are comparatively more frequent than those resulting in $H\beta$). Thus, the intrinsic line ratios applicable to HzPRGs are $H\alpha/H\beta = 3.1$ and $Ly\alpha/H\alpha = 16$ (Ferland & Osterbrock 1985; Osterbrock 1989).

The $H\beta$ emission line was not detected in any of the HzPRG spectra shown in Figure 1. Thus, the $Ly\alpha/H\alpha$ ratio must be used to calculate the extinction for individual sources. This ratio can be determined for four of eight sources; in the case of B3 0731+438 (~ 2.6) and 3C 257 (~ 0.1) by using data from Eales & Rawlings (1993)⁷, and in the case of TX 0200+015 (~ 1.7) and TX 0828+193 (~ 1.4) by using data from Table 2 and Röttgering et al. (1997). The average observed $Ly\alpha/H\alpha$ value determined for a larger sample of lower-redshift 3CR radio galaxies is ~ 1.5 (McCarthy 1988), and the observed $Ly\alpha/H\alpha$ ratio determined for two other $z > 2$ HzPRGs (Eales & Rawlings 1993) are ~ 1.4 (MRC 0406-24) and ~ 1.4 (53W002). All of the observed ratios are much less than the value of 16 expected for gas in a dust-free medium photoionized by a hard, nonthermal continuum.

The $E(B - V)$ values determined for the $z > 2$ HzPRGs B3 0731+438, 3C 257, MRC

⁷McCarthy et al. (1992) have also computed $Ly\alpha/H\alpha$ for B3 0731+438, as well as for the HzPRG MRC 0406-24. The discrepancy between the ratios determined by them and those determined by Eales & Rawlings (1993) arise from the fact that the former assume $H\alpha = H\alpha + [N II]$ and the latter assume $H\alpha = \frac{1}{2} (H\alpha + [N II])$.

0406-24, and 53W002 using data from Eales & Rawlings (1993) are in the range 0.11–0.76⁸. Using the H α measurements in Table 2, in combination with the Röttgering et al. (1997) Ly α measurements for TX 0200+015 and TX 0828+193, the $E(B - V)$ of these two galaxies was determined using the following procedure: Because the spectral resolution is sufficient to split the H α + [N II] λ 6583 complex, the values of H α have been determined using the three ratios of [N II] λ 6583 / H α plotted on Figure 3 (i.e., 0.19, 1.0, 3.74). The observed Ly α / H α line ratios were first corrected for Galactic extinction, then the extinction in the HzPRGs was determined assuming the extinction curves for the Milky Way (Savage & Mathis 1979), LMC (Nandy et al. 1981), and SMC (Prevot et al. 1984); the corresponding values of $E(B - V)$ are listed in Table 5. Given the redshift of the H α + [N II] λ 6548, 6583 complex and shape of the line emission, it seems quite unlikely that the [N II] λ 6583 / H α ratio is as high as 3.74. Thus, using the values from Table 5 and excluding values calculated assuming [N II] λ 6583 / H α = 3.74, feasible values of $E(B - V)$ range from 0.14 to 0.39. Such $E(B - V)$ values translate into $A_V \sim 0.5 - 1.0$ mag (depending on which extinction curve – Milky Way, SMC, LMC – is adopted) at the observed infrared wavelengths (i.e., rest-frame optical wavelengths of HzPRGs at $z = 2.2 - 2.6$), and a corresponding factor of ~ 2 reduction in the emission-line and continuum flux.

Although extinction is commonly determined using the luminous Ly α and H α emission lines (as done above), there are three concerns in using Ly α for such a measurement. These concerns and their relative applicability to the analysis of HzPRGs are summarized here. First, if there is a sufficient density of atomic hydrogen, the number of Ly α photons along

⁸This is the range of $E(B - V)$ for these sources assuming the extinction curves for the Milky Way, the Large Magellanic Cloud, and the Small Magellanic Cloud, and assuming an [N II] λ 6583 / H α ratio of 1.0 and 0.19. See the rest of the paragraph for a detailed explanation.

the line of sight can be greatly diminished by resonant scattering or associated absorption. One argument against this is that the measured Ly α emission-line widths are broad enough (\gtrsim few hundred km s $^{-1}$) such that most of the photons are in the wings of the line (McCarthy 1996). This can be understood if there exists a large velocity gradient across the gas that is being ionized - Ly α radiation emitted from gas at a given radius from the AGN passes through the gas farther out which is traveling at slower velocities because, to this gas, the Ly α photons do not appear to be resonant photons. However, recent medium resolution spectroscopy of 15 HzPRGs (van Ojik et al. 1997b), of which TX 0200+015 and TX 0828+193 are included, show evidence in favor of Ly α absorption. If the intrinsic Ly α profiles they fit to the observations are correct, the Ly α emission in these two galaxies may be diminished by up to 50%, making $E(B - V)$ lower by 0.10, 0.07, and 0.04 for models assuming a Milky Way, a LMC, and a SMC extinction curve, respectively. Second, if the gas is dense enough, Ly α photons can be destroyed by collisional de-excitation of the 2^2P state. This is because the Ly α photons must random walk out of the gas, and thus the lifetime of the 2^2P state is lengthened by the number of steps a Ly α photon must take to escape the gas. However, the densities required for the collisional de-excitation timescale to be shorter than the radiative de-excitation lifetime of the 2^2P state are in excess of 10^{10} cm $^{-3}$, a density only believed to be found in the densest areas of the broad-line region of AGNs (Osterbrock 1989). Third, if the alignment of the rest-frame UV morphology and the radio axis, as observed in many HzPRGs at $z > 0.5$, is the result of external illumination of gas and dust clouds by radiation from a central engine, these clouds most likely reflect the majority of the Ly α photons (e.g., McCarthy 1996). Given such a geometry, the Ly α luminosity would provide little information on the amount of dust present. However, such a process would also tend to raise, not lower, the Ly α /H α ratio from its intrinsic value, which is the opposite of what is observed.

5.5. Broad Lines

None of the eight HzPRGs at $z = 2.2 - 2.6$ were found to have broad emission-line cores (see Figure 1), nor do they appear to have broad emission-line wings. However, it is entirely possible that the cosmological distances of these galaxies may simply limit the ability to detect such a feature with 2–4 meter-class telescopes. The emission-line spectrum of the lower redshift HzPRG 3C 22 suggests that this may indeed be the case.

Figure 2 shows that the $H\alpha + [N\ II] \lambda\lambda 6548, 6583$ complex for 3C 22 has a line core width, $\Delta v_{\text{FWHM}} \sim 1700 \text{ km s}^{-1}$, consistent with the higher redshift HzPRGs observed (see Table 2). This emission emanates from extended, low density gas some distance from the nucleus of the galaxy. However, note the very broad $H\alpha$ wings ($\Delta v_{\text{FWZI}} \sim 7600 \text{ km s}^{-1}$) in 3C 22; such a feature is also visible in additional data (not shown here) from three KSPEC observing periods between 1994, July–September, and has also been reported by Economou et al. (1995) and Rawlings et al. (1995). Such a feature is indicative of the presence of a partially obscured Seyfert 1 nucleus, and is consistent with the hypothesis that FR II radio galaxies are quasars where the broad-line active nucleus is mostly obscured from the line of sight. The signal-to-noise ratio of the spectra of the higher redshift galaxies shown in Figure 1 is simply insufficient to rule out the presence of a similarly broad component in the $z = 2.2 - 2.6$ objects.

It is tempting to speculate that broad line wings, such as those observed in 3C 22, may be present in the more distant HzPRGs. However, current efforts using 2–4 meter-class telescopes suggests that larger aperture (i.e., 8–10 meter-class telescopes) will be required to detect broad line wings for HzPRGs at $z > 2$.

6. Summary

The following conclusions are drawn from the near-infrared spectroscopy of a sample of eight HzPRGs at $z = 2.2 - 2.6$:

1. For three of the eight HzPRGs, the emission-line ratios $[\text{O III}] \lambda 5007 / \text{H}\beta$ and $[\text{S II}] \lambda 6724 / \text{H}\alpha$ are characteristic of Seyfert 2 emission, consistent with the spectral type of the majority of low-redshift, narrow-line, powerful radio galaxies. The $[\text{O III}] \lambda 5007 / \text{H}\beta$ and $[\text{S II}] \lambda 6724 / \text{H}\alpha$ ratios and/or limits are inconclusive for the remaining five HzPRGs. Furthermore, of the six galaxies for which both H - and K -band spectra have been obtained, all six have observed $[\text{O III}] \lambda 5007 / (\text{H}\alpha + [\text{N II}] \lambda \lambda 6548, 6583)$ ratios consistent with Seyfert 2 ionization.
2. Unlike the emission-line spectra of low-redshift, narrow-line, powerful radio galaxies, the emission lines of the eight HzPRGs appear to contribute from $\sim 25\text{--}85\%$ of the H - and/or K -band light from these galaxies.
3. The southwestern component of TX 0828+193 shows no evidence of strong emission lines and comparatively strong continuum emission, whereas the northeastern component shows strong line emission and no noticeable continuum emission. If this featureless component is at the redshift of the radio galaxy, the continuum emission in TX 0828+193SW may be illumination from an AGN residing in the NW component. Alternatively, the AGN may reside in the SW component and thus ionize gas in the NW component, creating the strong lines observed. A comparison of these data with low-redshift, radio galaxies with off-nuclear knots supports the latter interpretation.
4. The observed $\text{Ly}\alpha / \text{H}\alpha$ ratios of the two TX sources are ~ 1.5 , much less than the value of 16 expected for gas photoionized by a hard nonthermal continuum. The discrepancy is most likely due to extinction by dust, though associated absorption may account for up to a

50% reduction in $\text{Ly}\alpha$. The ratio $\text{Ly}\alpha / \text{H}\alpha \sim 1.5$ corresponds to $A_V \sim 0.5 - 1.0$ (depending on which extinction curve – Milky Way, SMC, LMC – is used), and a corresponding factor of ~ 2 reduction in emission-line and continuum flux.

5. None of the eight HzPRGs at $z = 2.2 - 2.6$ have broad emission-line cores, and it is not clear whether any have broad emission-line wings. However, the near-infrared spectrum of 3C 22, a radio galaxy at $z = 0.937$ with $1 \mu\text{m}$ luminosity comparable to that of the eight HzPRGs at $z = 2.2 - 2.6$ and a radio luminosity only 3–5 times less, shows direct evidence for broad $\text{H}\alpha$ emission wings. Given that 3C 22 is at $\sim 1/3$ the luminosity distance of the other galaxies observed, systematic searches for broad emission-line wings in radio galaxies at $z > 2$ should be pursued, but may require the use of 8–10 meter-class telescopes.

These new data, along with recent rest-frame UV-to-optical polarimetry of HzPRGs, are consistent with the idea that many HzPRGs are predominantly ionized by an active nucleus, and that significant fraction of their SED may be due to non-thermal emission from the AGN.

It is a pleasure to thank the staffs of the UH 2.2m telescope and the United Kingdom Infrared Telescope for their generous support during these observations. D. Sanders, E. Egami, J. Hora, M. Dickinson, D. Kim, D. Jewitt, T. Greene, J. Deane, J. Goldader, A. Stockton, J. Jensen, G. Canalizo, and M. Shepherd provided useful discussions and assistance, and T. Soifer, L. Armus, and G. Neugebauer provided photometry from unpublished Keck data. I am also indebted to D. Jewitt for providing UKIRT observing time for TX 0828+193, G. Knopp for providing the H -band image of TX 0828+193, and J. Surace for obtaining the K' -band image of 4C 40.36. I also thank K. Teramura for making final adjustments to the figures presented in this paper, and the referee, A. Dey, for many useful comments. This research was supported in part by NASA grants NAGS-1741 and NAGW-3938.

A. Near-Infrared Finder Charts

Much of the difficulty in carrying out a HzPRG spectroscopy program on 2–4 meter-class telescopes is aligning the galaxy and the slit; the galaxies are often too faint to see after short integrations with an imaging array (UH 2.2m) and too faint to “peak up” on with the spectrometer (UKIRT). With the exception of the KSPEC observations of 3C 22, the galaxies were observed by first blind-offsetting from a star whose position is known to fair accuracy, or by placing the slit on the sky relative to bright stars in the field of view. The latter method is preferable to large offsets, and it also makes it straightforward to check whether or not the galaxy has drifted out of the slit because the positions of the stars in the field can constantly be monitored.

To aid in future observations of these galaxies, K' images of eight of the nine galaxies discussed in this paper have been taken (Figure 5). Also included in Figure 5 is an H -band image of TX 0828+193 from Knopp & Chambers (1997), which, though the field of view is much smaller than the K' images, shows the distinct double component morphology (see §5.3). A summary of the imaging observations is given in Table 6. All of the K' images of the $z > 2$ HzPRGs have been smoothed 4x4 pixels to make it easier to see the HzPRGs and other faint sources in the field. When there was some question as to which source was the HzPRG, the radio coordinates of the galaxy were used to perform astrometry with stars visible in the STScI Digitized Sky Survey⁹ images.

⁹The Digitized Sky Survey were produced at the Space Telescope Science Institute under the U.S. Government grant NAG W-2166. The images of these surveys are based on photographic data obtained using the Oschin Schmidt Telescope on Palomar Mountain and the UK Schmidt Telescope.

Table 1. Journal of Spectroscopic Observations

Source	B1950.0		z	Telescope	Instr.	P.A.	Aperture	$\frac{\lambda}{\Delta\lambda}$ ^a	samp	Date	band	Time ^b
	R.A.	Dec.										
TX 0200+015	02:00:08.20	01:34:45.95	2.232	UH 2.2m	KSPEC	133	0.8×2.0	760	1×1	09/93	H-K	0.3
				UKIRT	CGS4	133	1.5×6.0	860	3×2	10/94	K	2.2
				UH 2.2m	KSPEC	0	1.0×0.7	650	1×1	11/95	H-K	2.5
B3 0731+438	07:31:41.12	43:50:59.0	2.429	UH 2.2m	KSPEC	0	0.8×2.0	760	1×1	03/94	H-K	1.7
				UH 2.2m	KSPEC	0	1.0×2.0	620	1×1	12/94	H-K	2.1
				UKIRT	CGS4	0	2.5×4.9	430	4×2	10/95	K	1.2
TX 0828+193	08:28:01.22	19:23:23.8	2.572	UKIRT	CGS4	44	1.2×9.8	860	4×2	02/96	H,K	1.2,2.0
3C 257	11:20:34.55	05:46:46	2.482	UKIRT	CGS4	0	2.5×7.4	860	4×2	04/96	K	1.8
MG 1744+18	17:44:55.34	18:22:10.8	2.284	UKIRT	CGS4	56	1.2×4.9	860	4×2	05/95	K	1.4
4C 40.36	18:09:19.42	40:44:38.9	2.270	UKIRT	CGS4	80	1.5×6.0	860	6×1	08/93	K ^c	3.9
4C 48.48	19:31:40.03	48:05:07.1	2.344	UH 2.2m	KSPEC	0	0.8×4.0	760	1×1	07/93	J-H-K	2.6
				UKIRT	CGS4	32	1.5×6.0	860	6×1	08/93	K	6.9
4C 23.56	21:05:00.96	23:19:37.7	2.480	UKIRT	CGS4	52	1.5×6.0	860	6×1	08/93	K	9.6
				UKIRT	CGS4	52	1.5×6.0	860	3×2	10/94	H,K	1.2,3.6
Other:												
3C 22	00:48:04.73	50:55:44.8	0.937	UH 2.2m	KSPEC	0	1.0×2.0	620	1×1	12/94	J-H-K	1.2

^aAt $2.2 \mu\text{m}$

^bOn-Source Time

^cH-band observations of 4C 40.36 were obtained by Iwamuro et al. (1996) using the UH 2.2m telescope equipped with a OH-airglow supression spectrograph.

Table 2. Emission-Line Properties

Source	Instr.	Date	Line	λ_{obs}	$\frac{f(\lambda)}{f(\text{H}\alpha + [\text{N II}])}$	$f(\lambda)$	FWHM	S/N
		m/y		(μm)		(Watts m^{-2})	(km s^{-1})	
TX 0200+015	KSPEC	09/93	[O III] λ 5007	1.6183	1.1	...	1080	4.2
			H α + [N II]	2.1215	1.0	...	1040	3.6
	CGS4	10/94	H α + [N II]	2.1211	1.0	2.0×10^{-18}	1800	15
			[S II] λ 6724	2.1715	0.16	3.3×10^{-19}	1200	4.8
	KSPEC	11/95	[O III] λ 5007	1.6195	1.2	(2.4×10^{-18})	860	5.6
			H α + [N II]	2.1221	1.0	...	2000	5.9
B3 0731+438	KSPEC	3–12/94	[O III] λ 5007	1.7191	2.7	...	680	8.1
			[O I] λ 6300	...	<0.19	...	(1000)	...
			H α + [N II]	2.2542	1.0	...	870	5.1
			[O I] λ 6300	...	<0.08	...	(1000)	...
	CGS4	10/95	H α + [N II]	2.2489	1.0	...	1600	21
			[S II] λ 6724	2.3024	0.27	...	1180	12
TX 0828+193	CGS4	02/96	H β	...	<0.36	$< 6.5 \times 10^{-19}$	(1000)	...
			[O III] λ 5007	1.7885	1.4 ^a	2.5×10^{-18}	1300	6.9
			H α + [N II]	2.3463	1.0	1.8×10^{-18}	800	5.0
			[S II] λ 6724	...	<0.23	$< 4.2 \times 10^{-19}$	(1000)	...
3C 257	CGS4	04/96	[O I] λ 6300	...	<0.11	$< 3.0 \times 10^{-19}$	(1000)	...
			H α + [N II]	2.2857	1.0	2.6×10^{-18}	1750	6.9
			[S II] λ 6724	2.3429	0.20	5.2×10^{-19}	1180	3.2
MG 1744+18	CGS4	05/95	H α + [N II]	2.1552	1.0	...	1750	7.1
			[S II] λ 6724	...	<0.14	...	(1200)	...
4C 40.36	CGS4	08/93	[O I] λ 6300	...	<0.15	$< 5.2 \times 10^{-19}$	(1000)	...

Table 2—Continued

Source	Instr.	Date	Line	λ_{obs}	$\frac{f(\lambda)}{f(\text{H}\alpha + [\text{N II}])}$	$f(\lambda)$	FWHM	S/N
		m/y		(μm)		(Watts m^{-2})	(km s^{-1})	
			H α + [N II]	2.1462	1.0	3.4×10^{-18}	1660	7.1
			[S II] λ 6724	2.1945	0.35	1.2×10^{-18}	1320	4.6
4C 48.48	KSPEC	07/93	[O II] λ 3727	1.2462	0.37	...	1130	3.1
			H β	...	<0.26	...	(1000)	...
			[O III] λ 5007	1.6745	1.8	(6.0×10^{-18})	640	10
			[O I] λ 6300	...	<0.12	...	(1000)	...
			H α + [N II]	2.1945	1.0	...	1240	7.7
			[S II] λ 6724	2.2501	<0.12	...	(1200)	...
	CGS4	08/93	[O I] λ 6300	...	<0.05	$< 1.8 \times 10^{-19}$	(1000)	...
			H α + [N II]	2.1920	1.0	3.5×10^{-18}	1110	18
			[S II] λ 6724	2.2440	0.26	9.2×10^{-19}	1240	6.2
4C 23.56	CGS4	08/93	H α + [N II]	2.2830	1.0	1.2×10^{-18}	1520	5.9
		10/94	H β	...	<1.7	$< 5.9 \times 10^{-18}$	(1000)	...
			[O III] λ 5007	1.7442	1.3 ^a	4.4×10^{-18}	420	5.0
			[O I] λ 6300	...	<0.09	$< 3.2 \times 10^{-19}$	(1000)	...
			H α + [N II]	2.2861	1.0	3.4×10^{-18}	1280	6.8
			[S II] λ 6724	...	<0.14	$< 4.6 \times 10^{-19}$	(1200)	...
Other:								
3C 22	KSPEC	12/94	H β	...	<0.07	...	(1000)	...
			[O III] λ 5007	0.9696	0.76	...	940	5.6
			H α + [N II]	1.2712 ^b	1.0	...	1730	16
				1.2746 ^c				
			[S II] λ 6724	1.3015	0.07	...	880	4.0
			[O I] λ 6300		<0.02	...	(1000)	...
			He I λ 10830	2.0996	0.15	...	1660	8.6

Table 2—Continued

Source	Instr.	Date	Line	λ_{obs}	$\frac{f(\lambda)}{f(\text{H}\alpha + [\text{NII}])}$	$f(\lambda)$	FWHM	S/N
		m/y		(μm)		(Watts m^{-2})	(km s^{-1})	

^aFor TX 0828+193 and 4C 23.56, [O III] and H α + [N II] were not observed simultaneously, so the relative fluxes may be affected by blind offset errors.

^bObserved wavelength of H α λ 6563.

^cObserved wavelength of [N II] λ 6583.

Note. — All upper limits are 3σ based on the *rms* of the given spectrum and the adopted FWHM (in parentheses). [O III] fluxes in parentheses are adopted values based on the CGS4 H α flux for the radio galaxy and $f([\text{OIII}]\lambda 5007)/f(\text{H}\alpha + [\text{NII}])$ measured with KSPEC.

Table 3. Observed Emission-Line Ratios of HzPRGs & Low-z Galaxies

Source	$\frac{[\text{OIII}]\lambda 5007}{\text{H}\alpha + [\text{NII}]}$	$\frac{[\text{SII}]\lambda 6724}{\text{H}\alpha + [\text{NII}]}$	$\frac{\text{H}\alpha}{[\text{SII}]\lambda 6724}$	$\frac{\text{H}\alpha}{[\text{NII}]\lambda\lambda 6548 + 6583}$	$\frac{[\text{NII}]\lambda\lambda 6548 + 6583}{[\text{SII}]\lambda 6724}$
HzPRG	1.6 ± 0.6	0.25 ± 0.07
LzPRG	0.99 ± 0.34	0.27 ± 0.06	1.6 ± 0.6	0.74 ± 0.22	2.2 ± 0.4
Seyfert2	0.80 ± 0.40	0.18 ± 0.07	0.98 ± 0.45	3.0 ± 1.0	3.5 ± 1.7
LINER	0.062 ± 0.044	0.25 ± 0.08	0.71 ± 0.25	1.8 ± 0.6	2.6 ± 0.7
HII	0.068 ± 0.080	0.17 ± 0.04	1.7 ± 0.4	3.9 ± 0.8	2.4 ± 0.7

Table 4. Emission-Line Contribution to Infrared Flux

Source	Band	Magnitude ^a	Line/Total ^b (%)
TX 0200+015	<i>H</i>	18.90±0.05	25±2
TX 0200+015	<i>K</i>	18.27±0.03	28±2
4C 40.36	<i>K</i>	18.01±0.07	44±6
4C 23.56	<i>H</i>	19.73±0.10	98±21
	<i>K</i>	18.95±0.07	77±13

^aThese broad-band magnitudes are determined with the same apertures used for the spectroscopic observations (Table 1).

^bCalculation of line contribution to the broad-band magnitude of the HzPRGs, where the magnitudes are determined from imaging data by L. Armus (private communication).

Table 5. Color-Excess Calculations

Source	$\frac{[\text{N II}]}{\text{H}\alpha}$ ^a	$\frac{\text{Ly}\alpha}{\text{H}\alpha}$ ^b		Intrinsic $E(B-V)$ ^c		
		obs	corr	MW	LMC	SMC
TX 0200+015	0.19	1.0±0.1	1.0±0.1	0.38±0.02	0.26±0.02	0.18±0.01
	1.00	1.7±0.2	1.7±0.2	0.31±0.02	0.21±0.02	0.14±0.01
	3.74	4.0±0.6	4.0±0.6	0.19±0.02	0.13±0.01	0.09±0.01
TX 0828+193	0.19	0.86±0.19	0.95±0.2	0.39±0.03	0.27±0.02	0.18±0.02
	1.00	1.4±0.3	1.6±0.3	0.32±0.03	0.22±0.02	0.15±0.01
	3.74	3.4±0.7	3.8±0.8	0.20±0.03	0.14±0.02	0.09±0.02

^a1.0 = most probable value (Eales & Rawlings 1993), 0.19–3.74 = extreme values

^bLy α /H α observed and corrected for Galactic extinction.

^cCalculated color-excess assuming a Milky Way, LMC, and SMC extinction curve and corrected Ly α /H α .

Table 6. Journal of Imaging Observations

Source	Telescope	Instr.	Pixel Scale arcsec/pixel	Band	Date m/y	Time min.
TX 0200+015	UH 2.2m	QUIRC1024x1024	0.1886	K'	12/95	106
B3 0731+438	UH 2.2m	QUIRC1024x1024	0.1886	K'	12/95	40
TX 0828+193 ^a	UKIRT	IRCAM3	0.286	H	03/96	160
3C 257	UH 2.2m	QUIRC1024x1024	0.1886	K'	04/96	20
MG 1744+18	UH 2.2m	QUIRC1024x1024	0.1886	K'	07/97	45
4C 40.36	UH 2.2m	QUIRC1024x1024	0.06084	K'	07/97	56
4C 48.48	UH 2.2m	QUIRC1024x1024	0.1886	K'	12/95	28
4C 23.56	UH 2.2m	QUIRC1024x1024	0.1886	K'	12/95	40
3C 22	UH 2.2m	QUIRC1024x1024	0.1886	K'	12/95	18

^aThe *H*-band image of TX0828+193 is taken from Knopp & Chambers (1997).

REFERENCES

- Baldwin, J. A., Phillips, M. M., & Terlevich, R. 1981, *PASP*, 93, 5
- Blair, W. P. & Fesen, R. A. 1994, *ApJ*, 424, L103
- Chambers, K. C., Miley, G. K., van Breugel, W. J. M. 1988. *ApJ*, 327, L47
- Chambers, K. C., Miley, G. K., van Breugel, W. J. M., Bremer, M. A. R., Huang, J.-S., & Trentham, N. A. 1996, *ApJS*, 106, 247
- Chini, R., & Krügel, E. 1994, *A&A*, 288, L33
- Cimatti, A., Dey, A., van Breugel, W., Antonucci, R., Spinrad, H. 1996, *ApJ*, 465, 145
- Costero, R. & Osterbrock, D. E. 1977, *ApJ*, 211, 675
- Dey, A. & Spinrad, H. 1996, *ApJ*, 459, 133
- Dey, A., Spinrad, H., & Dickinson, M. 1995, *ApJ*, 440, 515
- Dey, A., van Breugel, W., Vacca, W., & Antonucci, R. 1997, *ApJ*, in press
- Djorgovski, S., Spinrad, H., Pedelty, J., Rudnick, L., & Stockton, A. 1987, *AJ*, 93, 1307
- Downes, D., Solomon, P. M., Sanders, D. B., & Evans, A. S. 1996, *A&A*, 313, 91
- Dunlop, J. S. Hughes, D. H., Rawlings, S., Eales, S., & Ward, M. J. 1994, *Nature*, 370, 347
- Dunlop, J. S. & Peacock, J. A. 1993, *MNRAS*, 263, 936
- Eales, S. A. & Rawlings, S. 1993, *ApJ*, 411, 67
- Eales, S. A. & Rawlings, S. 1996, *ApJ*, 460, 68
- Economou, F., Lawrence, A., Ward, M. J., Blanco, P. R. 1995, *MNRAS*, 272, L5

- Evans, A. S. 1996, Ph.D. Thesis, University of Hawaii
- Evans, A. S., Sanders, D. B., Mazzarella, J. M., Solomon, P. M., Downes, D., Kramer, C., & Radford, S. J. E. 1996, *ApJ*, 457, 658
- Ferland, G. J. & Osterbrock, D. E. 1985, *ApJ*, 289, 105
- Golombek, D., Miley, G. K., & Neugebauer, G. 1988, *AJ*, 95, 26
- Grandi, S. A. 1977, *ApJ*, 215, 446
- Hammer, F., Le Fèvre, & Proust 1991, *ApJ*, 374, 91
- Hughes, D., Dunlop, J. S., & Rawlings, S. 1997, *MNRAS*, 289, 766
- Hodapp, K., Hora, J. L., Irwin, E., & Young, T. 1994, *PASP*, 106, 87
- Impey, C. & Gregorini, L. 1993, *AJ*, 105, 853
- Iverson, R. J. 1995, *MNRAS*, 275, 33L
- Iwamuro, F., Oya, S., Tsukamoto, H., Maihara, T. 1996, *ApJ*, 466, L67
- Jim, K. T. C. 1997, *PASP*, in preparation
- Kim, D.-C., Sanders, D. B., Veilleux, S., Mazzarella, J. M., & Soifer, B. T. 1995, *ApJS*, 98, 129
- Knapp, G. R. & Patten, B. M. 1991, *AJ*, 101, 1609
- Knopp, G. 1997, Ph.D. Thesis, University of Hawaii
- Knopp, G. & Chambers, K. C. 1997, *ApJ*, in press
- Manzini, A. & di Serego Alighieri, S. 1996, *A&A*, 311, 79

- Mazzarella, J. M., Graham, J. R., Sanders, D. B., & Djorgovski, S. G. 1993, *ApJ*, 409, 170
- McCarthy, P. J. 1993, *ARA&A*, 31, 639
- McCarthy, P. J. 1996, in *Cold Gas at High Redshift*, eds. M. N. Bremer et al. (Dordrecht: Kluwer), p. 349
- McCarthy, P. J., Elston, R., & Eisenhardt, P. 1992, *ApJ*, 387, L29
- McCarthy, P. J., van Breugel, W. J. M., Spinrad, H., & Djorgovski, S. 1987, *ApJ*, 321, L29
- Mirabel, I. F., Sanders, D. B., & Kazès 1989, *ApJ*, 340, L9
- Nandy, K., Morgan, D. H., Willis, A. J., Wilson, R., Gondhalekar, P. M. 1981, *MNRAS*, 196, 955
- Osterbrock, D. E. 1989, *Astrophysics of Gaseous Nebulae and Active Galactic Nuclei* (California: University Science Books)
- Osterbrock, D. E. & Miller, J. S. 1975, *ApJ*, 197, 535
- Prevot, M. L., Lequeux, J., Maurice, E., Prevot, L., Rocca-Volmerang, B. 1984, *A&A*, 132, 389
- Rawlings, S., Eales, S. A., & Lacy, M. 1991, *MNRAS*, 251, 17
- Rawlings, S., Lacy, M., Sivia, D. S., & Eales, S. A. 1995, *MNRAS*, 274, 428
- Rawlings, S., Saunders, R. D. E., Eales, S. A., & Mackay, C. 1989, *MNRAS*, 240, 701
- Röttgering, H. J. A. 1993, PhD Thesis, Rijksuniversiteit te Leiden, The Netherlands
- Röttgering, H. J. A., Lacy, M., Miley, G. K., Chambers, K. C., & Saunders, R. 1994, *A&AS*, 108, 79

Röttgering, H. J. A., Miley, G. K., Chambers, K. C., & Macchetto, F. 1995, *A&AS*, 114, 51

Röttgering, H. J. A., van Ojik, R., Miley, G. K., Chambers, K. C., van Breugel, W. J. M., & de Koff, S. 1997, *A&A*, in press

Savage, B. D. & Mathis, J. S. 1979, *ARA&A*, 17, 73

Scoville, N. Z., Yun, M. S., Windhorst, R. A., Keel, W. C., Armus, L. 1997, *ApJ*, 485, L21

Tadhunter, C. N., Fosbury, R. A. E., Binette, L., Danziger, I. J., Robinson, A. 1987, *Nature*, 325, 504

van Breugel, W., Miley, G., Heckman, T., Butcher, H., Bridle, A. 1985, *ApJ*, 290, 496

van Ojik, R. 1995, PhD Thesis, Rijksuniversiteit te Leiden, The Netherlands

van Ojik, R. et al. 1997a, *A&A*, 321, 389

van Ojik, R., Röttgering, H. J. A., Miley, G. K., & Hunstead, R. W. 1997b, *A&A*, 317, 358

Veilleux, S., Kim, D.-C., Sanders, D. B., Mazzarella, J. M., & Soifer, B. T. 1995, *ApJS*, 98, 171

Veilleux, S. & Osterbrock, D. E. 1987, *ApJS*, 63, 295

Windhorst et al. 1991, *ApJ*, 380, 362

Figure Captions

Figure 1. Rest-frame optical spectroscopy for the sample of 8 HzPRGs at redshifts 2.2 to 2.6. (a) TX 0200+015; (b) B3 0731+438; (c) TX 0828+193; (d) 3C 257, MG 1744+18, 4C 40.36; (e) 4C 48.48; (f) 4C 23.56. The resolutions and the samplings of all of the observations are listed in Table 1. For the KSPEC observations, the pixel sampling for J , H , and K -bands are 12, 14, and 20 $\mu\text{m pixel}^{-1}$, respectively. For the CGS4 observations, the pixel samplings are as follows: 6.6 $\mu\text{m pixel}^{-1}$ for B3 0731+438, MG 1744+18, and TX 0828+193; 5.6 $\mu\text{m pixel}^{-1}$ for 4C 48.48, 4C 40.36, and the 1993, August observations of 4C 23.56; 11 $\mu\text{m pixel}^{-1}$ for TX 0200+015 and the 1994, October observations of 4C 23.56. The CGS4 spectra of TX 0200+015, 4C 40.36, and TX 0828+193SW (K band) have been smoothed an additional 10 pixels, 10 pixels, and 100 pixels, respectively.

Figure 2. Rest-frame 4800–10840 \AA spectroscopy of the radio galaxy 3C 22. The pixel sampling for J , H , and K -bands are 12, 14, and 20 $\mu\text{m pixel}^{-1}$, respectively. Note the broad $\text{H}\alpha$ wings.

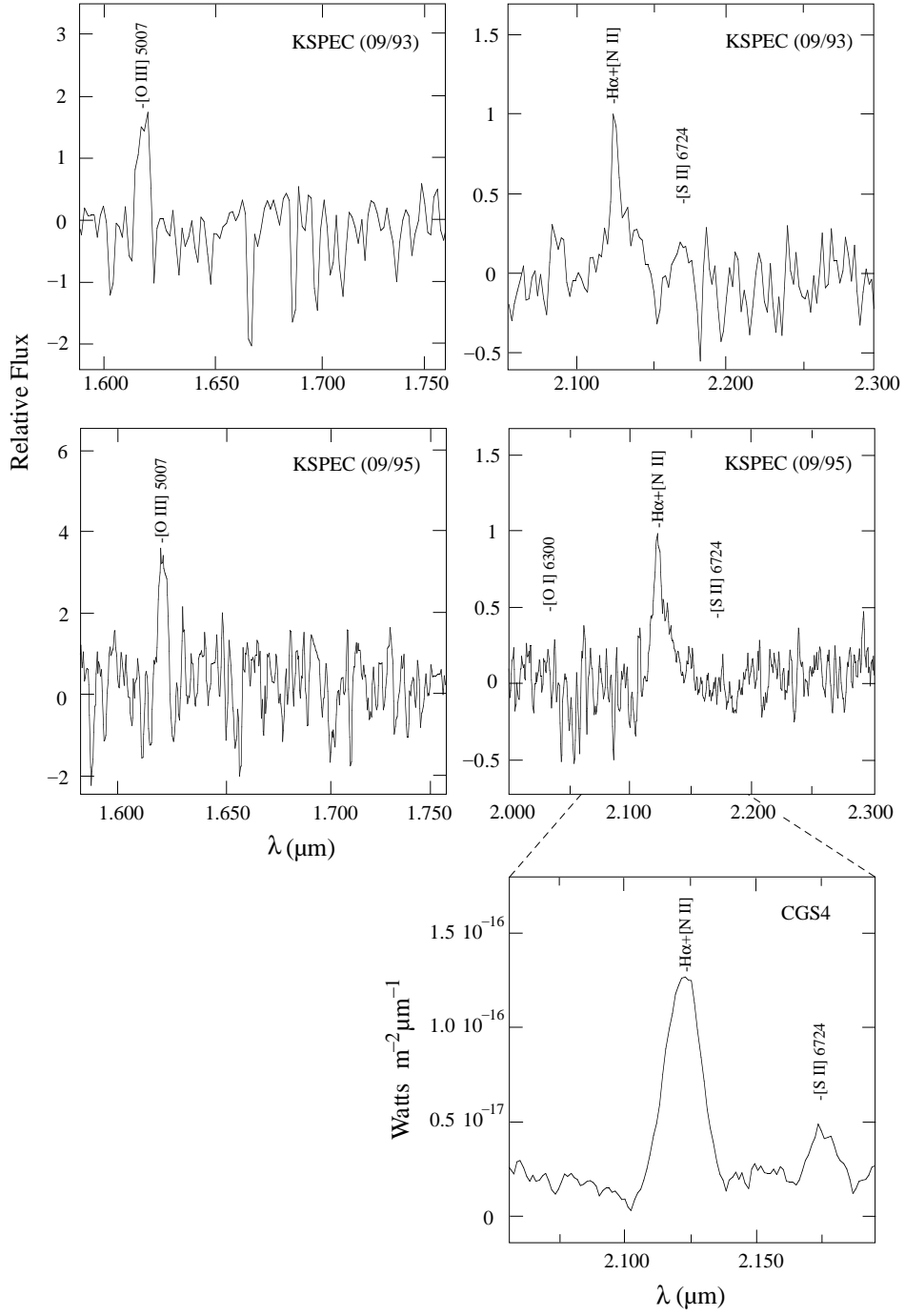
Figure 3. $\log ([\text{O III}] \lambda 5007 / \text{H}\beta)$ vs. $\log ([\text{S II}] \lambda 6724 / \text{H}\alpha)$ for 8 HzPRGs. For all of the data, the ratios are plotted assuming the lower limit value $[\text{N II}] \lambda 6583 / \text{H}\alpha = 0.19$. The two additional $[\text{N II}] \lambda 6583 / \text{H}\alpha$ ratios of 1.0 and 3.74 (see text) are indicated by the small solid circles on the thin lines.

Figure 4. a) $L_{[\text{O III}] \lambda\lambda 4959, 5007}$ vs. $P_{151\text{MHz}}$, adapted from Eales & Rawlings (1996). Symbols—(\bullet) sources from this paper, ($+$) objects in Eales & Rawlings (1996). The radio data for the TX galaxies discussed in this paper are determined from data in Röttgering (1993), and the radio data for the 4C sources and B3 0731+438 are determined from data in the NASA/IPAC Extragalactic Database (NED). The $[\text{O III}] \lambda\lambda 4959, 5007$ luminosities of TX 0200+015, B3 0731+438, and 4C 48.48 have been determined using

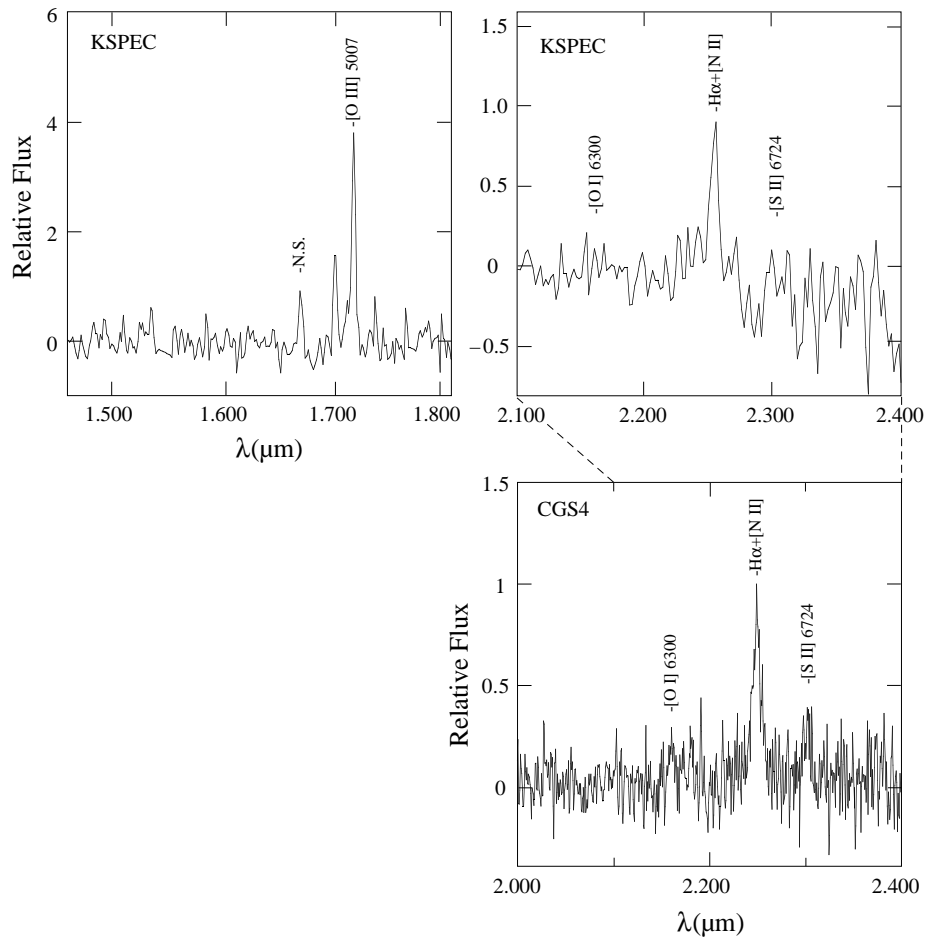
KSPEC observations of the $[\text{O III}] \lambda\lambda 4959, 5007 / \text{H}\alpha + [\text{N II}] \lambda\lambda 6548, 6583$ ratios and CGS4 measurements of $\text{H}\alpha + [\text{N II}] \lambda\lambda 6548, 6583$ luminosities (the $\text{H}\alpha + [\text{N II}] \lambda\lambda 6548, 6583$ luminosity of B3 0731+438 is the measured value from Eales & Rawlings 1993). b) $L_{[\text{OIII}] \lambda\lambda 4959, 5007} / P_{151\text{MHz}}$ vs. $P_{151\text{MHz}}$.

Figure 5. Near-infrared images of the nine HzPRGs discussed in the paper. A scale bar is provided in each image, and the identification is marked with two ticks. In all images, North is up, and East is to the left.

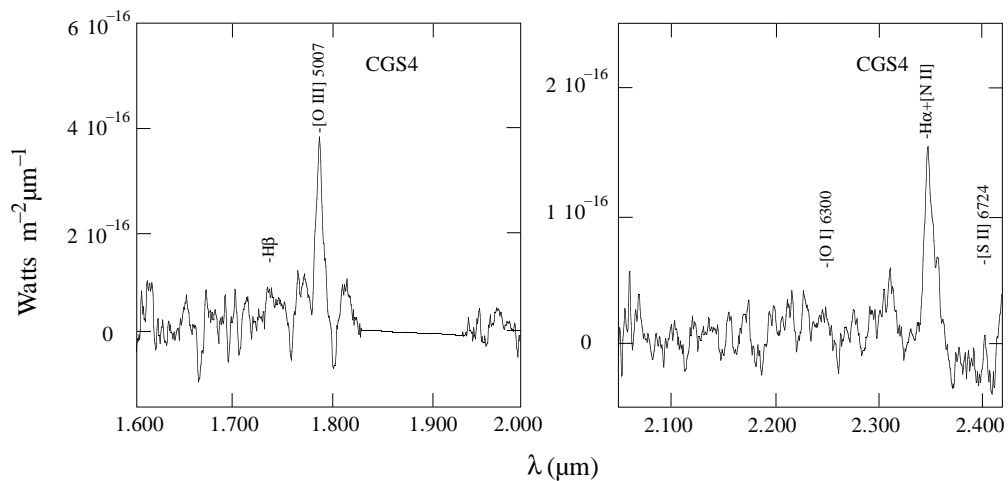
TX 0200+015



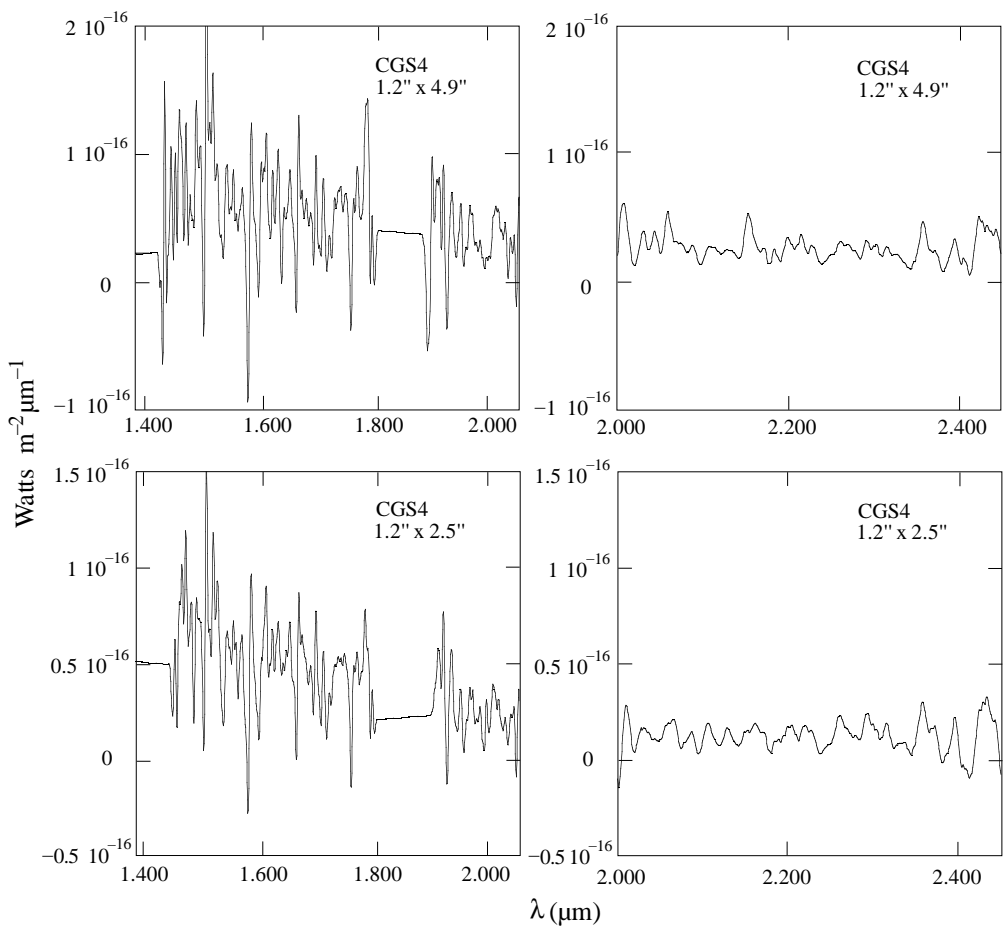
B3 0731+438



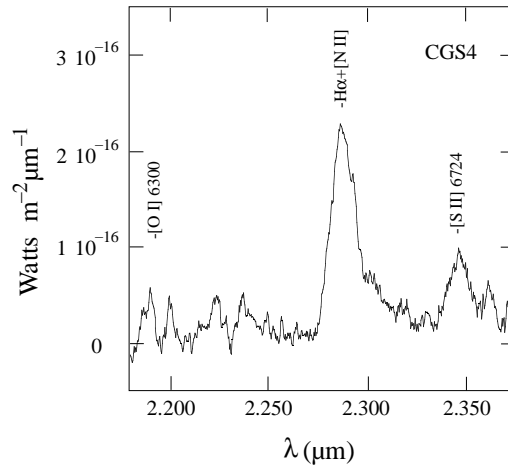
TX 0828+193 NE



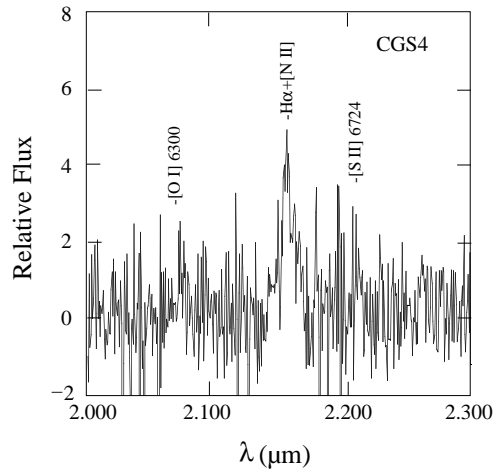
TX 0828+193 SW



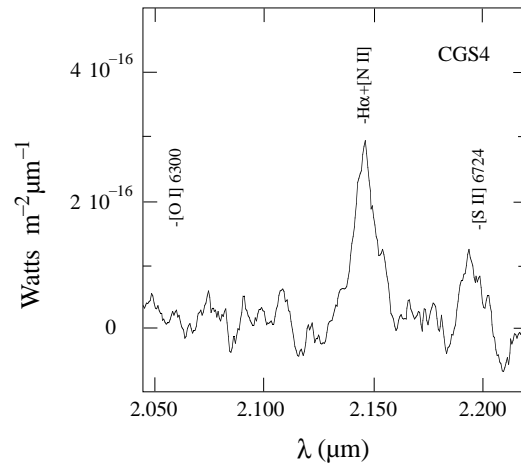
3C 257



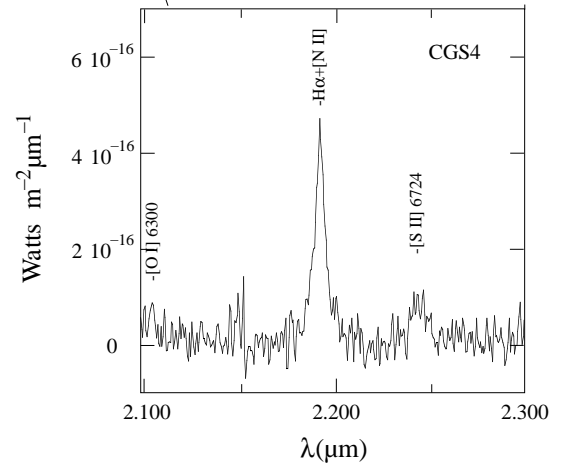
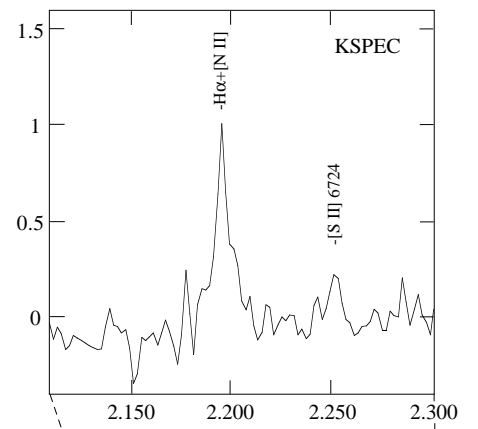
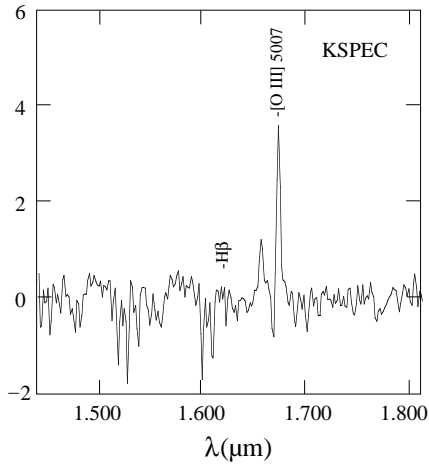
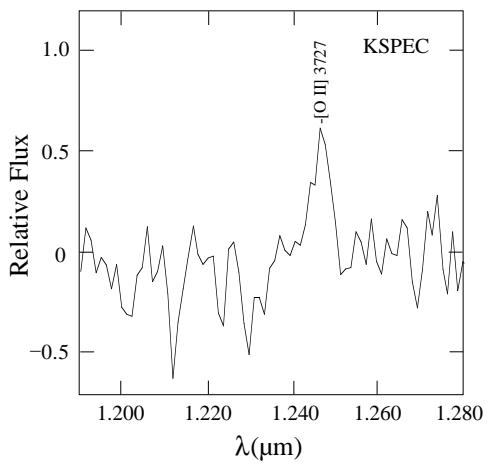
MG 1744+18



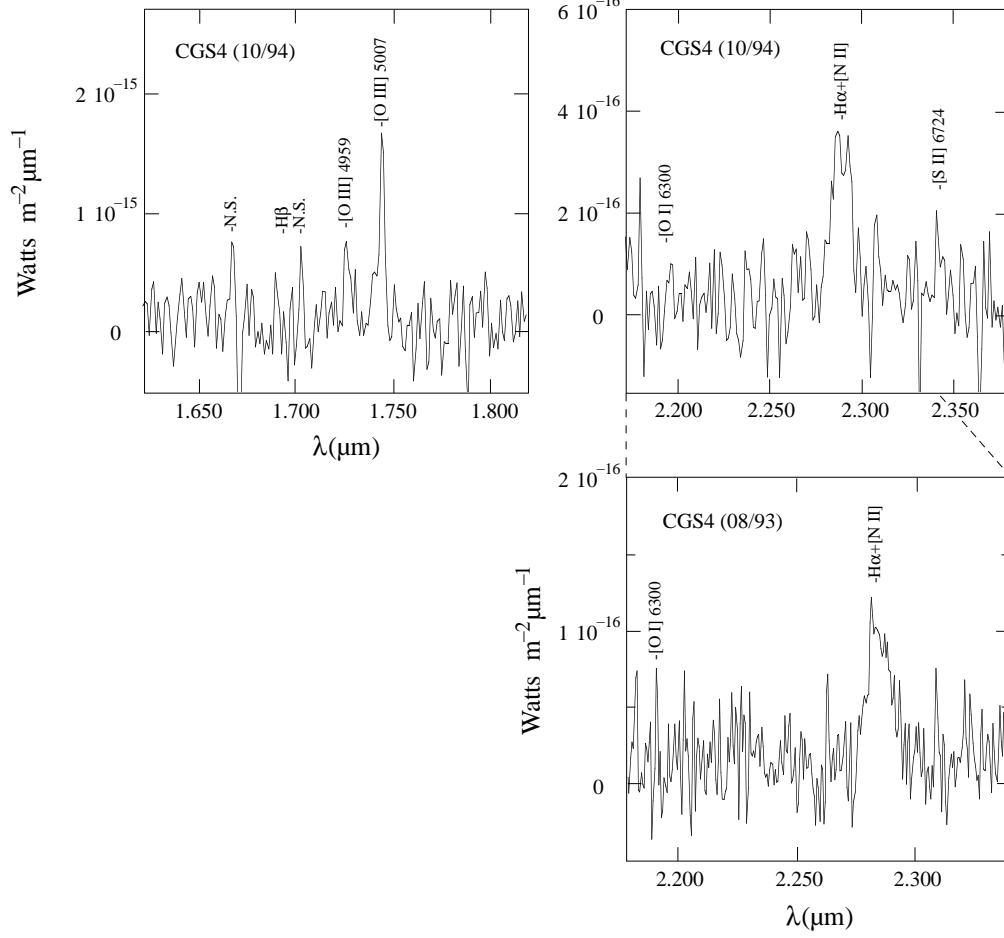
4C 40.36



4C 48.48



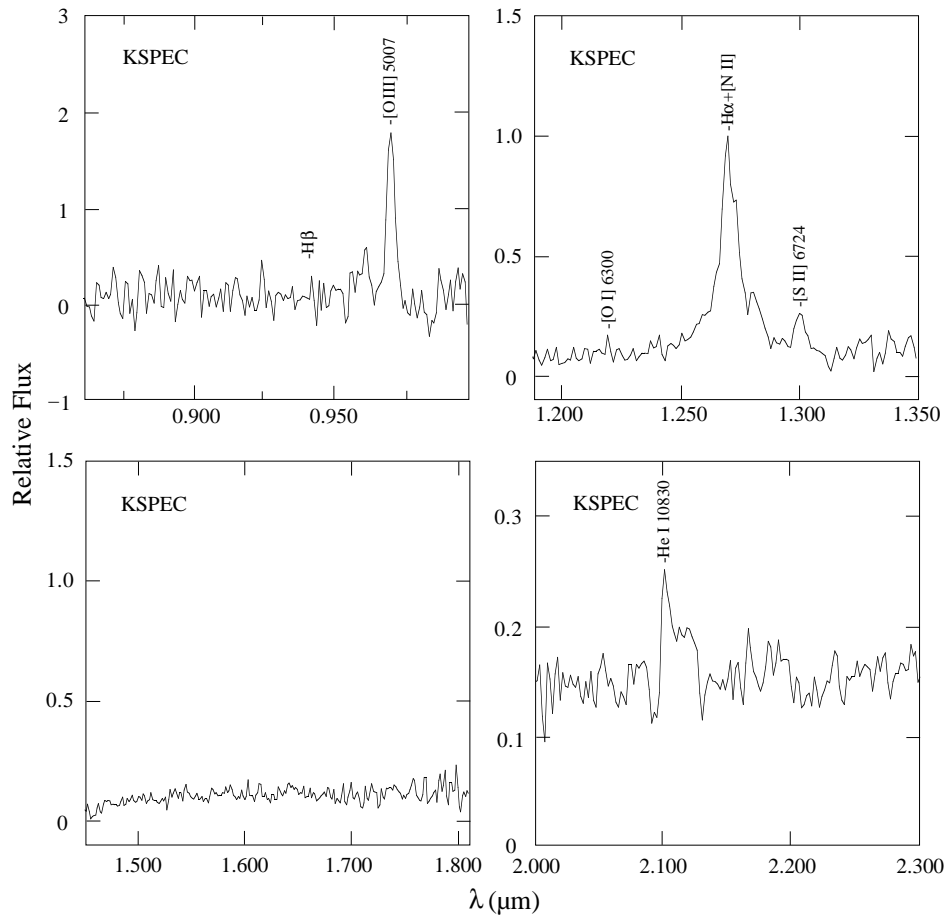
4C 23.56



This figure "asefig5_p1.gif" is available in "gif" format from:

<http://arxiv.org/ps/astro-ph/9802151v1>

3C 22



This figure "asefig5_p2.gif" is available in "gif" format from:

<http://arxiv.org/ps/astro-ph/9802151v1>

